



CHORUS

This is the accepted manuscript made available via CHORUS. The article has been published as:

Calculated transport properties of CdO: Thermal conductivity and thermoelectric power factor

L. Lindsay and D. S. Parker

Phys. Rev. B **92**, 144301 — Published 1 October 2015

DOI: [10.1103/PhysRevB.92.144301](https://doi.org/10.1103/PhysRevB.92.144301)

**Calculated transport properties of CdO: thermal conductivity and thermoelectric power
factor**

L. Lindsay and D. S. Parker

Materials Science and Technology Division, Oak Ridge National Laboratory, Oak Ridge,
Tennessee 37831, USA

This manuscript has been authored by UT-Battelle, LLC under Contract No. DE-AC05-00OR22725 with the U.S. Department of Energy. The United States Government retains and the publisher, by accepting the article for publication, acknowledges that the United States Government retains a non-exclusive, paid-up, irrevocable, world-wide license to publish or reproduce the published form of this manuscript, or allow others to do so, for United States Government purposes. The Department of Energy will provide public access to these results of federally sponsored research in accordance with the DOE Public Access Plan(<http://energy.gov/downloads/doe-public-access-plan>).

Calculated transport properties of CdO: thermal conductivity and thermoelectric power factor

L. Lindsay and D. S. Parker

Materials Science and Technology Division, Oak Ridge National Laboratory, Oak Ridge,
Tennessee 37831, USA

Abstract

We present first principles calculations of the thermal and electronic transport properties of the oxide semiconductor CdO. In particular, we find from theory that the accepted thermal conductivity κ value of $0.7 \text{ Wm}^{-1}\text{K}^{-1}$ is approximately one order of magnitude too small; our calculations of κ of CdO are in good agreement with recent measurements. We also find that alloying of MgO with CdO is an effective means to reduce the lattice contribution to κ , despite MgO having a much larger thermal conductivity. We further consider the electronic structure of CdO in relation to thermoelectric performance, finding that large thermoelectric power factors may occur if the material can be heavily doped *p*-type. This work develops insight into the nature of thermal and electronic transport in an important oxide semiconductor.

PACS: 66.70.-f, 63.20.Kr, 71.15.-m, 72.15.Jf, 44.10.+i, 63.20dk

I. INTRODUCTION

Knowledge of thermal and electronic transport properties of materials is of great interest for both fundamental scientific knowledge and practical applications. For example, characteristics of a myriad of semiconductors, including band gaps, band masses, conductivities (thermal and electrical), carrier mobility, and numerous other properties, are routinely available in standard reference handbooks [1, 2] that are used by researchers and industrial operations worldwide in such diverse areas as the automotive industry, microelectronics, and chemical supply. While such data are subject to revision as new information becomes available, the vast majority of such revisions are essentially incremental in scope, with slow changes with time in reported properties. For example, a measured direct band gap of 2.28 eV in the oxide semiconductor CdO was reported in 1975 by Koffyberg [3] and is repeated in a standard handbook reference [2]. Since then, a more recent measurement of this band gap gives a value of 2.16 eV [4], only nominally lower.

In this work we will discuss a situation in which a well-accepted material transport property – the lattice thermal conductivity $\kappa_{lattice}$ – of CdO is apparently understated in handbook references by *as much as an order of magnitude*. Like numerous other binary equiatomic semiconductors, *e.g.*, the lead chalcogenides and MgO, CdO forms in a rocksalt structure and heat is primarily carried by the lattice via phonons. Interest in CdO and its properties has developed recently in a diverse set of research applications including thin film transparent conductors [5], thermoelectrics [6, 7] and plasmonic materials [8]. The standard accepted value of κ for CdO is $0.7 \text{ Wm}^{-1}\text{K}^{-1}$ [1]. Given consideration, this is a surprisingly low value particularly for a simple binary oxide, for which high κ values are typical. ZnO, for example, is reported to have $\kappa=54 \text{ Wm}^{-1}\text{K}^{-1}$ [9], nearly two orders of magnitude larger. While CdO has a significantly heavier average atomic mass than ZnO, and hence lower Debye temperature thus favoring lower $\kappa_{lattice}$,

this is not nearly sufficient to account for this difference. The reported $0.7 \text{ Wm}^{-1}\text{K}^{-1}$ figure is in fact near the “minimum thermal conductivity” for this system [10], for which the phonon mean free paths (MFPs) approach a single lattice spacing.

In this work we will show, both from our own fully *ab initio* calculations of κ_{lattice} as well as an analysis of recently published thermoelectric transport data, that the true κ_{lattice} of CdO is much larger and likely falls between 5.6 and $9.3 \text{ Wm}^{-1}\text{K}^{-1}$. Note that owing to recent advances in computational power and numerical techniques, it is now possible to calculate κ_{lattice} from first principles *with no adjustable parameters* and in generally good agreement with measured values [11-17]. This work is among the first fully *ab initio* calculations of thermal conductivity in a semiconducting oxide, which present specific challenges to theory in the light of potential electronic correlations. Despite this, our results are in good agreement with available experimental results.

Although not the focus of this work, we also present electronic structure and Boltzmann transport calculations for CdO suggesting that if heavily doped *p*-type, CdO may show extremely large thermoelectric power factors at elevated temperatures. This is due largely to a highly favorable Fermi surface topology, in particular a network of two-dimensional features residing essentially at the valence band maximum. Such features present in the valence band of the high performance thermoelectric PbTe [18] have already been shown to be highly beneficial for thermoelectric performance [19].

The remainder of this paper is organized as follows: In Section II we present our calculations of the thermal conductivity of CdO, along with a discussion of recent thermal conductivity data on this material; in Section III we discuss the electronic structure *vis a vis* thermoelectric transport; and in Section IV we present our conclusions.

II. THERMAL CONDUCTIVITY OF CdO

We calculate the lattice thermal conductivity:

$$\kappa_{lattice} = \sum_{\vec{q}j} C_{\vec{q}j} v_{\vec{q}j}^2 \tau_{\vec{q}j} \quad (1)$$

as a sum over contributions from all phonon modes with wave vector \vec{q} in branch j . Diagonalization of the dynamical matrix gives the phonon frequencies $\omega_{\vec{q}j}$ needed to determine the specific heat $C_{\vec{q}j}$ and velocity $\vec{v}_{\vec{q}j}$ for each mode [20]. For the cubic crystals considered here the thermal conductivity tensor can be described by a single value and the velocity and transport lifetime $\tau_{\vec{q}j}$ components are in the heat transport direction parallel to a small applied temperature gradient. The transport lifetimes are determined from the full solution of the Peierls-Boltzmann equation for phonon transport with harmonic and third-order anharmonic (lowest order in perturbation theory) [20-22] interatomic force constants (IFCs) determined from density functional theory (DFT) [23, 24]. For the temperatures considered here the differences between this full solution and that given by the relaxation time approximation are negligible for CdO. We note that software is now publicly available for calculations of IFCs and phonon thermal transport for a variety of systems [25-27]. Here we give a brief description of the DFT and transport parameters relevant to the CdO $\kappa_{lattice}$ calculations, and leave further details to previously published work [13, 28-30].

Most IFC calculations were done within the local density approximation (LDA) using the publicly available Quantum Espresso (QE) software package [31, 32] with norm-conserving Martin-Troulliers pseudopotentials [33]. A 100 Ry energy cutoff for the electronic wave functions and 10x10x10 k-point meshes were used for the electronic structure calculations. The energy was minimized to determine the equilibrium lattice constant $a=4.694 \text{ \AA}$ for the CdO

rocksalt structure, in good agreement with the measured value of 4.689 Å [2]. Density functional perturbation theory [34] using a 6x6x6 q-point mesh was employed to determine the harmonic IFCs. The dielectric constant and Born effective charges were also determined using the QE package to give the long range Coulomb interactions important for describing the splitting of the longitudinal and transverse optic branches. The calculated phonon dispersion is in generally good agreement with available measured data. The anharmonic IFCs are determined from numerical derivatives using a series of Γ -point electronic structure calculations on supercells of 216 atoms systematically perturbed from the ground state [29, 30, 35]. Interactions were considered out to the fifth nearest neighbors of the unit cell atoms and all point group symmetries and translational invariance conditions were enforced [28-30]. Phonon scattering from naturally occurring isotopic mass variances was calculated via perturbation theory [36, 37] and input into the Boltzmann transport formalism using Matthiessen's rule [20]. IFC files and QE input files have been made available [38].

Figure 1 gives the calculated $\kappa_{lattice}$ of CdO with naturally occurring isotope concentrations (solid curve) as a function of temperature compared with measured κ data (blue [6, 7] and green [8] squares) and the room temperature reference handbook value (red square) [1]. Electronic transport properties were also characterized in Refs. 6-8 and the electronic contributions to the thermal conductivities, $\kappa_{electronic}$ (triangles), as determined from the Wiedemann-Franz law, were separated from the total κ . Surprisingly, the calculated $\kappa_{lattice}$ and measured room temperature κ values are all over an order of magnitude larger than the reference handbook value $\kappa=0.7 \text{ Wm}^{-1}\text{K}^{-1}$ [1] at room temperature. We have no explanation for this ultralow value. However, we note that it is not consistent with the simple CdO structure and phonon dispersion. The calculated $\kappa_{lattice}$ is in good agreement with the κ data of Li, *et. al.*, [7] over a broad temperature range.

Agreement with the measured $\kappa_{lattice}$ (circles) becomes best at higher temperatures where the anharmonic phonon-phonon scattering is stronger relative to possible extrinsic scattering mechanisms, *e.g.*, grain boundaries and defects. We note that phonon scattering from isotopic mass variance plays no significant role in determining $\kappa_{lattice}$ for CdO for $T > 200$ K as the intrinsic anharmonic scattering is much stronger.

Sachet, *et. al.* report a significantly lower $\kappa_{lattice} = 5.6 \text{ Wm}^{-1}\text{K}^{-1}$ [8] compared to Li, *et. al.* [7]. We note that using the generalized gradient approximation (GGA) our calculations also give $\kappa_{lattice}$ lower than LDA, $\kappa_{lattice} = 5.76 \text{ Wm}^{-1}\text{K}^{-1}$, due to lower frequency optic phonons and thus more scattering of the heat-carrying acoustic phonons. The thermorefectance κ measurements of Sachet, *et. al.*, were done on thin film samples (0.4-0.5 μm thick) doped with Dy (5×10^{19} - $1 \times 10^{21} \text{ cm}^{-3}$ concentrations) with significant native O vacancy defect concentrations. The grain sizes of the treated commercial CdO powder of Ref. 7 were 5-10 μm and also expected to have natural native O vacancy concentrations. We tested the effects of finite sample size and Dy substitutional and O vacancy defects on the calculated $\kappa_{lattice}$ of CdO. The defect scattering was modeled as a simple mass variance perturbation exactly as the isotope scattering [36, 37]. Even at the highest concentrations reported in Ref. 8, the calculated room temperature $\kappa_{lattice}$ was not sensitive to the mass variance of the Dy dopants and O vacancies, being reduced by only 0.32% and 0.13%, respectively. However, as discussed in Ref. 8, the lattice distortions around the defects may play a more significant role in determining $\kappa_{lattice}$. Using Green's function calculations, Katcho, *et. al.*, [39] found that vacancies in diamond can enhance the phonon scattering cross section of vacancies by a factor of ten over simple mass variance.

The size dependence of $\kappa_{lattice}$ was estimated using an empirical boundary scattering term, $\tau_{\vec{q}j}^{-1, boundary} = |\vec{v}_{\vec{q}j}| / L$, [20] where L gives a measure of grain or system size. This is of particular

relevance for thermoelectric performance as nanostructuring has proven an effective method for reducing $\kappa_{lattice}$ and enhancing thermoelectric figures of merit in other materials [40, 41]. The dashed black curve in Fig. 1 gives the calculated $\kappa_{lattice}$ with boundary scattering for $L=5 \mu\text{m}$. This gives improved agreement with the measured $\kappa_{lattice}$ from Ref. 7 for a sample having similar grain sizes. As expected, boundary scattering is relatively weak compared to intrinsic anharmonic scattering at high T and plays a more significant role in determining $\kappa_{lattice}$ as temperature decreases. For $L=0.4 \mu\text{m}$ the calculated room temperature $\kappa_{lattice}=7.16 \text{ Wm}^{-1}\text{K}^{-1}$ is in substantially better agreement with the $5.6 \text{ Wm}^{-1}\text{K}^{-1}$ value of Ref. 8 with comparable film thickness. Phonons at very low frequency with large MFPs, particularly the longitudinal acoustic modes, give $\sim 10\%$ of the total $\kappa_{lattice}$ and their contributions are truncated by the boundary scattering. Acoustic phonons with $\text{MFP} < 0.5 \mu\text{m}$ give the dominant contributions to $\kappa_{lattice}$. We note that optic phonon contributions to $\kappa_{lattice}$ are non-negligible at room temperature, giving $\sim 8\%$ of the total. This often occurs in materials with low phonon frequency scales with thermally populated optic modes and dispersive optic branches, *e.g.*, in Mg_2Si , Mg_2Sn [28], PbSe and PbTe [14].

We also characterized the effect of alloying CdO with another rocksalt material MgO , an important constituent of the Earth's mantle. MgO has a much larger calculated room temperature $\kappa_{lattice}=59.14 \text{ Wm}^{-1}\text{K}^{-1}$ [42], ~ 6 times higher than that of CdO , and in good agreement with measured data [43]. Phonon-isotope scattering from the naturally occurring isotope concentrations were included. The higher $\kappa_{lattice}$ of MgO is partly due to the lighter Mg mass and partly due to stronger interatomic bonding as suggested by the smaller lattice constant and larger IFCs of MgO . These give higher acoustic phonon velocities and higher lying optic branches, the later leads to larger acoustic lifetimes due to reduced scattering with higher

frequency optic modes. We used a virtual crystal approximation in which the harmonic and anharmonic properties (*e.g.*, IFCs, lattice constants, masses) are averaged in proportion to the concentration of the constituent Cd and Mg elements to model the alloy $\text{Cd}_{1-x}\text{Mg}_x\text{O}$ properties. Phonon scattering from the alloy mass disorder is treated in the same manner as isotope scattering, and disorder in the harmonic and anharmonic IFCs is neglected. This virtual crystal approximation worked well previously in describing κ of $\text{Mg}_2\text{Si}_x\text{Sn}_{1-x}$ [28].

Figure 2 gives the calculated room temperature κ_{lattice} of $\text{Cd}_{1-x}\text{Mg}_x\text{O}$ as a function of Mg concentration x . Surprisingly, despite increasing phonon frequencies of the virtual crystal, the room temperature κ_{lattice} of $\text{Cd}_{1-x}\text{Mg}_x\text{O}$ initially decreases from that of CdO with increasing Mg concentration, attaining a minimum value nearly half the κ_{lattice} of CdO and more than 12 times reduced from that of MgO for $x=0.2$. At 1000K the competing effects of mass disorder and increasing phonon frequencies initially give non-monotonic behavior with increasing x , however, κ_{lattice} generally increases in going from pure CdO to pure MgO.

III. ELECTRONIC STRUCTURE AND THERMOELECTRIC TRANSPORT IN CdO

Although the basic electronic structure of CdO is well-known (see Refs. 44-54 for more information) we present here a brief summary for reference. All results in this section were characterized using the linearized augmented plane wave (LAPW) code WIEN2K [55], using an augmentation of the GGA [56] known as a modified Becke Johnson potential [57], which yields band gaps much closer to experiment than those calculated in the GGA, which generally understates band gaps and in fact predicts metallic behavior for CdO [45]. LAPW sphere radii of 2.4 Bohr for O and 2.37 Bohr for Cd were employed, and the self-consistent calculations used approximately 2000 k-points in the full fcc Brillouin zone. RK_{max} was set to 9.0, where R is the O sphere radius and K_{max} is the largest plane-wave vector. The transport calculations used

approximately 10000 k-points. Our band-structure results are consistent with those of Ref. 54, which also used the modified Becke-Johnson method.

Depicted in Figure 3 is the calculated band structure of CdO. We find a calculated indirect band gap of 1.65 eV, with the conduction band minimum at the Γ point and the valence band maximum at the L point. Both band edge locations are as experimentally observed, while the calculated direct band gap of 2.91 eV is somewhat larger than the measured values of 2.16-2.28 eV [3, 4]. However, this band gap overstatement proves not of serious consequence. We have checked the transport calculations with a “scissors shift” calculation with the indirect band gap reduced to 1 eV, with no change to the thermopower results in the relevant doping and temperature ranges. We also note band degeneracy at the L point and a comparatively small dispersion in the valence band, both generally favorable for thermoelectric performance.

In Figure 4 we depict the calculated electronic density-of-states (DOS) of CdO. There is some hybridization, with the valence band being mainly Cd and the much lighter conduction band a mixture of Cd and O. Of most interest here, however, is the extremely rapid increase in the DOS just below the VBM, reaching nearly $2/(\text{eV}\cdot\text{unit cell})$ (note there is one formula unit per cell) only 100 meV below the VBM. This is suggestive of a large effective mass, and it is well known that, at constant carrier concentration, the thermopower is proportional to the effective mass. In order to understand this behavior, in Figure 5 we plot the isoenergy, or Fermi surface, of CdO for the $T=0$ Fermi level taken 70 meV into the valence band. This figure shows a bowed two-dimensional cylindrical feature necking out from the L-points and connecting with similar features from the other L points. All told there are twelve of these cylinders, roughly forming the edges of a cube inscribed within the fcc Brillouin zone. One recalls that an exactly two dimensional cylinder has a step function DOS, and while these cylinders are not perfectly two

dimensional the near-vertical band edge in the DOS plot emphasizes this two dimensional quality. Similar cylinders were found theoretically in the valence band of PbTe [18]. Despite lying 0.25 eV into the valence band in that material, they are believed to substantially contribute to the exceptional thermoelectric performance, or ZT , measured. Here, however, the cylindrical features fall virtually at the band edge and can therefore be expected to even more strongly enhance thermoelectric transport.

To assess this, in Figure 6 we plot the calculated $T=800$ K thermopower S (computed within the constant scattering time approximation, see Ref. 58 for details of this approximation) versus calculated conductivity (with respect to an unknown scattering time), compared with the known high performance thermoelectrics PbTe and PbSe. One recalls that high ZT requires both high thermopower and high electrical conductivity *simultaneously*. We see that while the n -type performance of CdO is likely less than that of PbTe and PbSe, the p -type CdO may exhibit very large power factors. In fact in the region in which S varies between 200 and 300 μVK^{-1} (the typical thermopower range for a high- ZT material), the σ/τ of CdO is twice, or more, larger than that for PbTe. This doping range corresponds to a hole concentration of 0.023-0.077 holes/unit cell, or $p=8.9\times 10^{20} - 2.9\times 10^{21} \text{ cm}^{-3}$. These results are noteworthy given that in this temperature range optimized PbTe exhibits a ZT value of 2.2 [59], among the highest of any bulk material. While one cannot exclude scattering time differences, or the generally lower thermal conductivity of PbTe, from this comparison, it suggests that p -type CdO may be of considerable interest as a thermoelectric material.

We note that CdO generally forms n -type, so that it will be a significant experimental challenge to attain the required p -type doping. Nevertheless, there is precedent for the practicality of p -type doping of oxide systems. ZnO, for example, was for many years found only

to form *n*-type, but there is now a substantial body of experimental work [60-64] suggesting the possibility of *p*-type doping in ZnO. We anticipate a similar scenario for CdO, with the most likely potential *p*-type dopants being the monovalent alkali metals.

IV. SUMMARY AND CONCLUSIONS

Using a rigorous first principles Peierls-Boltzmann transport equation approach we have demonstrated that the lattice thermal conductivity $\kappa_{lattice}$ of CdO is more than an order of magnitude larger than the reported handbook value [1], and in agreement with recent measurements [6-8]. The dependence of the calculated $\kappa_{lattice}$ on temperature, impurities, boundaries and alloying with MgO was shown and discussed. Despite the higher thermal conductivity of MgO, alloying CdO with this material can reduce the CdO $\kappa_{lattice}$ by ~ 2 times, perhaps giving improved thermoelectric performance. Other relevant thermoelectric properties of CdO were also calculated and discussed, including a demonstration that the thermoelectric power factor of *p*-type CdO may outperform that of PbTe for certain temperatures and carrier concentrations. CdO may be an important material for a range of applications, *e.g.*, thin film transparent conductivity, plasmonics and thermoelectrics. Accurate knowledge of the fundamental transport parameters of CdO, including $\kappa_{lattice}$, is important for determining the utility of this material for such purposes.

Acknowledgements

L. L. acknowledges support from the U. S. Department of Energy, Office of Science, Office of Basic Energy Sciences, Materials Sciences and Engineering Division. D. P. acknowledges the support of the S3TEC Energy Frontier Research Center.

References

- [1] W. M. Haynes and D. R. Lide, *CRC Handbook of Chemistry and Physics: A Ready-Reference Book of Chemical and Physical Data* (CRC, Boca Raton, 2010).
- [2] W. Martienssen and H. Warlimont, *Springer Handbook of Condensed Matter and Materials Data* (Springer, Heidelberg, 2005).
- [3] F. P. Koffyberg, *Phys. Rev. B* 13, 4470 (1976).
- [4] P. H. Jefferson, S. A. Hatfield, T. D. Veal, P. D. C. King, C. F. McConville, J. Zúñiga-Pérez, and V. Muñoz-Sanjosé, *Appl. Phys. Lett.* 92, 022101 (2008).
- [5] K. M. Yu, M. A. Mayer, D. T. Speaks, H. He, R. Zhao, L. Hsu, S. S. Mao, E. E. Haller, and W. Walukiewicz, *J. of Appl. Phys.* 111, 123505 (2012).
- [6] L. Li, S. Liang, S. Li, J. Wang, S. Wang, G. Dong, and G. Fu, *Nanotech.* 25, 425402 (2014).
- [7] Q. Lu, S. Wang, L. Li, J. Wang, S. Dai, W. Yu, and G. Fu, *Science China: Phys., Mech. and Astro.* 57, 1644 (2014).
- [8] E. Sachet, C. T. Shelton, J. S. Harris, B. E. Gaddy, D. L. Irving, S. Curtarolo, B. F. Donovan, P. E. Hopkins, P. A. Sharma, A. L. Sharma, J. Ihlefeld, S. Franzen, and J.-P. Maria, *Nat. Mat.* 14, 414 (2015).
- [9] G. A. Slack, *Phys. Rev. B* 6, 3791 (1972).
- [10] D. G. Cahill, S. K. Watson, and R. O. Pohl, *Phys. Rev. B* 46, 6131 (1992).
- [11] D. A. Broido, M. Malorny, G. Birner, N. Mingo, and D. A. Stewart, *Appl. Phys. Lett.* 91, 231922 (2007).
- [12] A. Ward, D. A. Broido, D. A. Stewart and G. Deinzer, *Phys. Rev. B* 80, 125203 (2009).
- [13] L. Lindsay, D. A. Broido, and T. L. Reinecke, *Phys. Rev. Lett.* 109, 095901 (2012).

- [14] Z. Tian, J. Garg, K. Esfarjani, T. Shiga, J. Shiomi, and G. Chen, Phys. Rev. B 85, 184303 (2012).
- [15] L. Lindsay, D. A. Broido, and T. L. Reinecke, Phys. Rev. Lett. 111, 025901 (2013).
- [16] L. Lindsay, W. Li, J. Carrete, N. Mingo, D. A. Broido, and T. L. Reinecke, Phys. Rev. B 89, 155426 (2014).
- [17] G. Fugallo, A. Cepellotti, L. Paulatto, M. Lazzeri, N. Marzari, and F. Mauri, Nano Lett. 14, 6109 (2014).
- [18] D. J. Singh, Phys. Rev. B 81, 195217 (2010).
- [19] D. Parker, X. Chen, and D. J. Singh, Phys. Rev. Lett. 110, 146601 (2013).
- [20] J. M. Ziman, *Electrons and Phonons* (Oxford University Press, London, 1960).
- [21] M. Omini and A. Sparavigna, Physica B 212, 101 (1995).
- [22] M. Omini and A. Sparavigna, Phys. Rev. B 53, 9064 (1996).
- [23] P. Hohenberg and W. Kohn, Phys. Rev. 136, B864 (1964).
- [24] W. Kohn and L. J. Sham, Phys. Rev. 140, A1133 (1965).
- [25] Wu Li, J. Carrete, N. A. Katcho, and N. Mingo, Comp. Phys. Comm. 185, 1747 (2014).
- [26] A. Togo, L. Chaput, and I. Tanaka, Phys. Rev. B 91, 094306 (2015).
- [27] A. Chernatynskiy and S. R. Phillpot, Comp. Phys. Comm. 192, 196 (2015).
- [28] W. Li, L. Lindsay, D. A. Broido, D. A. Stewart, and N. Mingo, Phys. Rev. B 86, 174307 (2012).
- [29] L. Lindsay, D. A. Broido, and T. L. Reinecke, Phys. Rev. B 87, 165201 (2013).
- [30] N. Mingo, D. A. Stewart, D. A. Broido, L. Lindsay, and W. Li, “*Ab initio thermal transport in Length-Scale Dependent Phonon Interactions*,” (Springer, 2014).

- [31] P. Giannozzi, S. Baroni, N. Bonini, M. Calandra, R. Car, C. Cavazzoni, D. Ceresoli, G. L. Chiarotti, M. Cococcioni, I. Dabo, A. D. Corso, S. Gironcoli, S. Fabris, G. Fratesi, R. Gebauer, U. Gerstmann, C. Gougoussis, A. Kokalj, M. Lazzeri, L. Martin-Samos *et al.*, *J. Phys.: Condens. Matter* 21, 395502 (2009).
- [32] <http://www.quantum-espresso.org>.
- [33] N. Troullier and J. L. Martins, *Phys. Rev. B* 43, 1993 (1991).
- [34] S. Baroni, S. Gironcoli, A. D. Corso, and P. Giannozzi, *Rev. Mod. Phys.* 73, 515 (2001).
- [35] K. Esfarjani and H. T. Stokes, *Physical Review B* 77, 144112 (2008).
- [36] S. I. Tamura, *Phys. Rev. B* 30, 849 (1984).
- [37] L. Lindsay, D. A. Broido, and T. L. Reinecke, *Phys. Rev. B* 88, 144306 (2013).
- [38] Supplemental material made available for calculations.
- [39] N. A. Katcho, J. Carrete, W. Li, and N. Mingo, *Phys. Rev. B* 90, 094117 (2014).
- [40] D. J. Singh and I. Terasaki, *Nat. Mat.* 8, 616 (2008).
- [41] A. J. Minnich, M. S. Dresselhaus, Z. F. Ren, and G. Chen, *Energy Environ. Sci.* 2, 466 (2009).
- [42] L. Lindsay, D. A. Broido, J. Carrete, N. Mingo, and T. L. Reinecke, *Phys. Rev. B* 91, 121202(R) (2015).
- [43] D. A. Dalton, W.-P. Hsieh, G. T. Hohensee, D. G. Cahill, and A. F. Goncharov, *Sci. Rep.* 3, 2400 (2013).
- [44] J. Robertson and B. Falabretti, “*Electronic structure of transparent conducting oxides*,” *Handbook of Transparent Conductors*, pg. 27, e.d. D. S. Ginly (Springer, 2010).
- [45] M. Burbano, D. O. Scanlon, and G. W. Watson, *J. Am. Chem. Soc.* 133, 15065 (2011).
- [46] J. E. Jaffe, Ravindra Pandey, and A. B. Kunz, *Phys. Rev. B* 43, 14030 (1991).

- [47] Y. Z. Zhu, G. D. Chen, Honggang Ye, Aron Walsh, C. Y. Moon, and Su-Huai Wei, *Phys. Rev. B* 77, 245209 (2008).
- [48] Y. Dou, R. G. Egdell, D. S. L. Law, N. M. Harrison, and B. G. Searle, *J. of Phys.: Cond. Mat.* 10, 8447 (1998).
- [49] P. D. C. King, Tim D. Veal, A. Schleife, J. Zúñiga-Pérez, B. Martel, P. H. Jefferson, F. Fuchs, V. Muñoz-Sanjosé, F. Bechstedt, and Chris F. McConville, *Phys. Rev. B* 79, 205205 (2009).
- [50] K. Maschke and U. Rössler, *Physica Stat. Sol. (b)* 28, 577 (1968).
- [51] L. F. J. Piper, Alex DeMasi, Kevin E. Smith, A. Schleife, F. Fuchs, F. Bechstedt, J. Zuniga-Pérez, and V. Munoz-Sanjosé, *Phys. Rev. B* 77, 125204 (2008).
- [52] A. Schleife, F. Fuchs, J. Furthmüller, and F. Bechstedt, *Phys. Rev. B* 73, 245212 (2006).
- [53] A. Janotti, David Segev, and Chris G. Van de Walle, *Phys. Rev. B* 74, 045202 (2006).
- [54] H. Dixit, R. Saniz, Stefaan Cottenier, D. Lamoen, and B. Partoens, *J. of Phys.: Cond. Mat.* 24, 205503 (2012).
- [55] P. Blaha, K. Schwarz, G. Madsen, D. Kvasnicka and J. Luitz, *WIEN2k*, An Augmented Plane Wave + Local Orbitals Program for Calculating Crystal Properties (Karlheinz Schwarz, Techn. Universität Wien, Austria), 2001. ISBN 3-9501031-1-2.
- [56] J. P. Perdew, K. Burke, and M. Ernzerhof, *Phys. Rev. Lett.* 77, 3865 (1997).
- [57] F. Tran and P. Blaha, *Phys. Rev. Lett.* 102, 226401 (2009).
- [58] D. Parker, M.-H. Du, and D. J. Singh, *Phys. Rev. B* 83, 245111 (2011).
- [59] K. Biswas, J. He, I. D. Blum, C.-I. Wu, T. P. Hogan, D. N. Seidman, V. P. Dravid, and M. G. Kanatzidis, *Nature* 489, 414 (2012).

- [60] D. C. Look, D. C. Reynolds, C. W. Litton, R. L. Jones, D. B. Eason, and G. Cantwell, *Appl. Phys. Lett.* 81, 1830 (2002).
- [61] K. K. Kim, H. S. Kim, D. K. Hwang, J. H. Lim, and S. J. Park, *Appl. Phys. Lett.* 83, 63 (2003).
- [62] M. Joseph, H. Tabata, H., and T. Kawai, *Japanese J. of Appl. Phys.* 38(11A), L1205 (1999).
- [63] Y. R. Ryu, T. S. Lee, and H. W. White, *Appl. Phys. Lett.* 83, 87 (2003).
- [64] F. X. Xiu, Z. Yang, L. J. Mandalapu, D. T. Zhao, J. L. Liu, and W. P. Beyermann, *Appl. Phys. Lett.* 87, 152101 (2005).

Figure Captions

Figure 1: The calculated $\kappa_{lattice}$ of CdO versus temperature with naturally occurring isotope concentrations (solid black curve). The dashed black curve gives $\kappa_{lattice}$ with boundary scattering included, $L=5\mu\text{m}$, consistent with the measured data in Refs. 6 and 7. Experimental κ data from Li, *et. al.*, [6, 7] and Sachet, *et. al.*, [8] are given by blue and green symbols, respectively. Squares give measured κ values, triangles give $\kappa_{electronic}$ calculated from the Wiedemann-Franz law and electronic transport measurements and circles give the subsequent $\kappa_{lattice}$. Also shown is the reference handbook κ value (filled red square) [1].

Figure 2: The calculated $\kappa_{lattice}$ of $\text{Cd}_{1-x}\text{Mg}_x\text{O}$ versus Mg concentration x at $T=300\text{K}$ (black circles) and $T=1000\text{K}$ (red circles).

Figure 3: The calculated electronic band structure of CdO. Energy zero is set to the valence band maximum.

Figure 4: The calculated electronic density-of-states of CdO. Energy zero is set to the valence band maximum.

Figure 5: The calculated isoenergy surface of CdO for E_F taken 70 meV into the valence band.

Figure 6: The calculated thermopower S vs. conductivity σ/τ for CdO and the high performance thermoelectrics PbTe and PbSe.

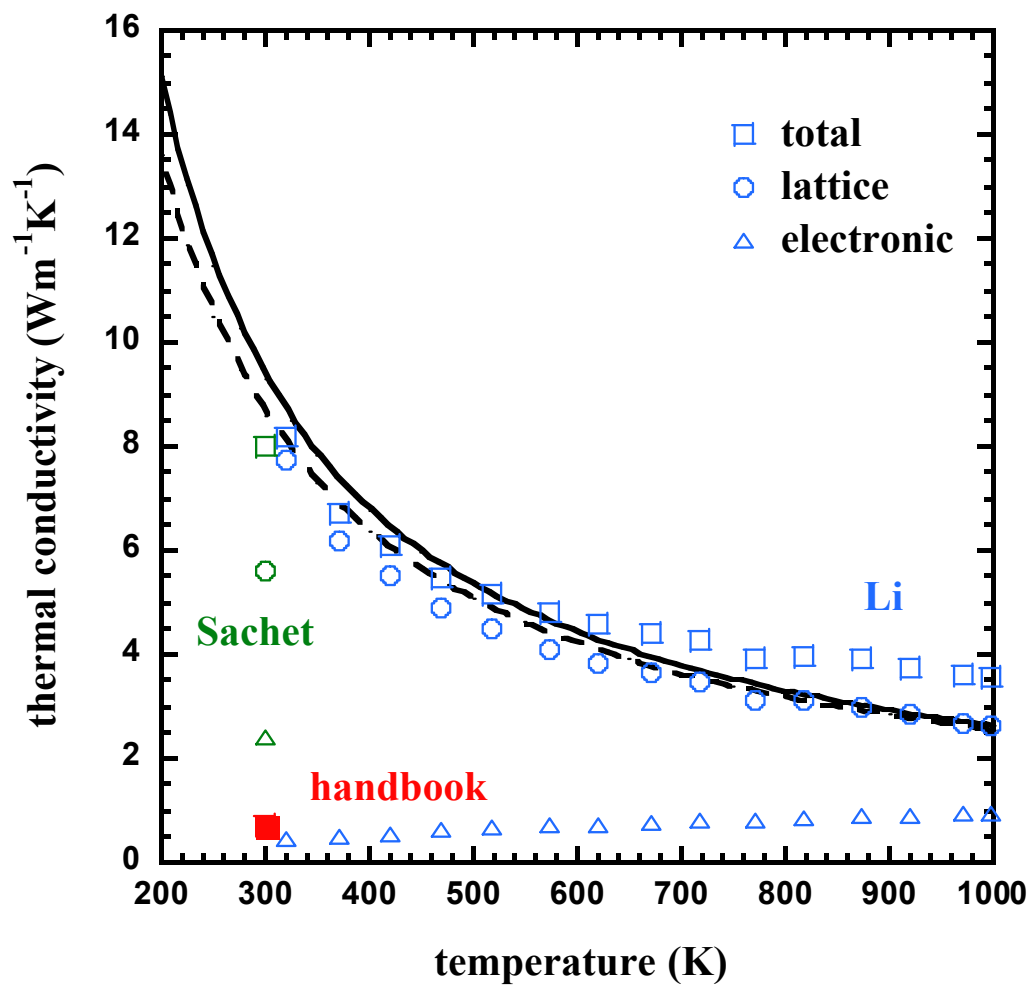


Figure 1

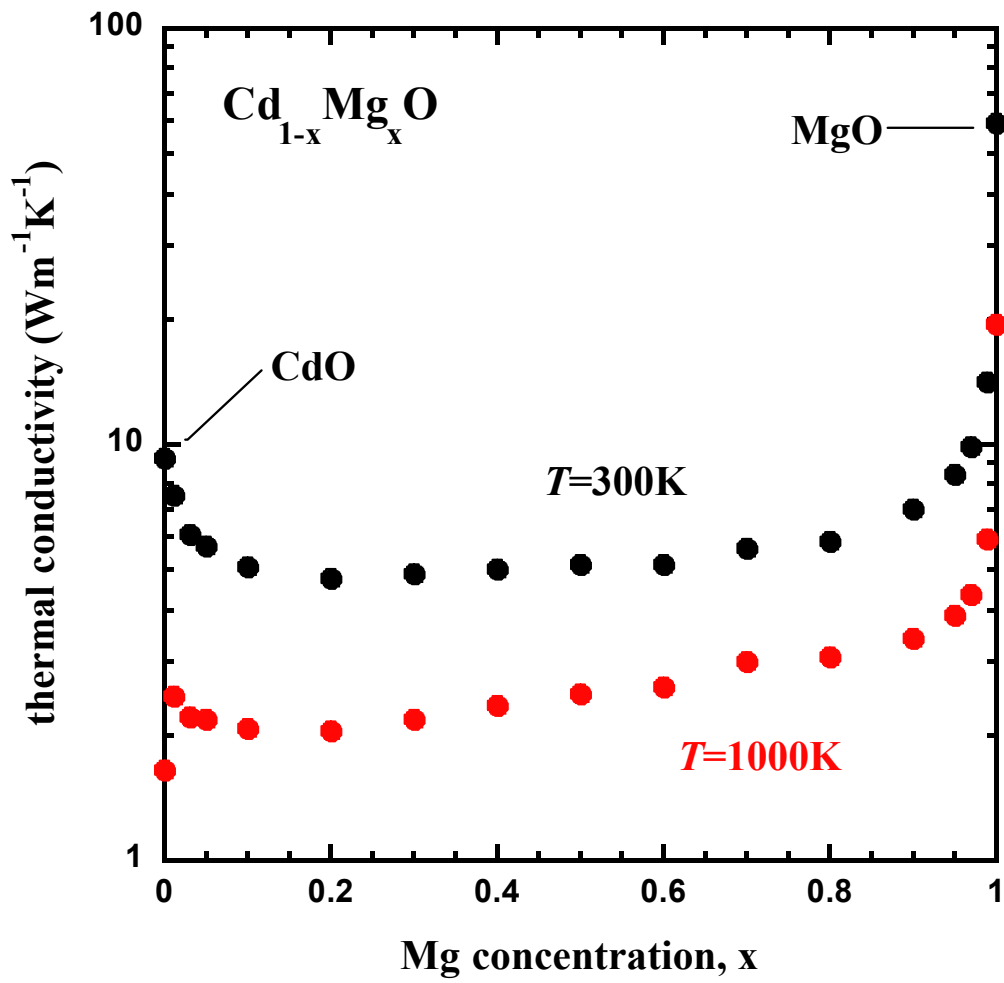


Figure 2

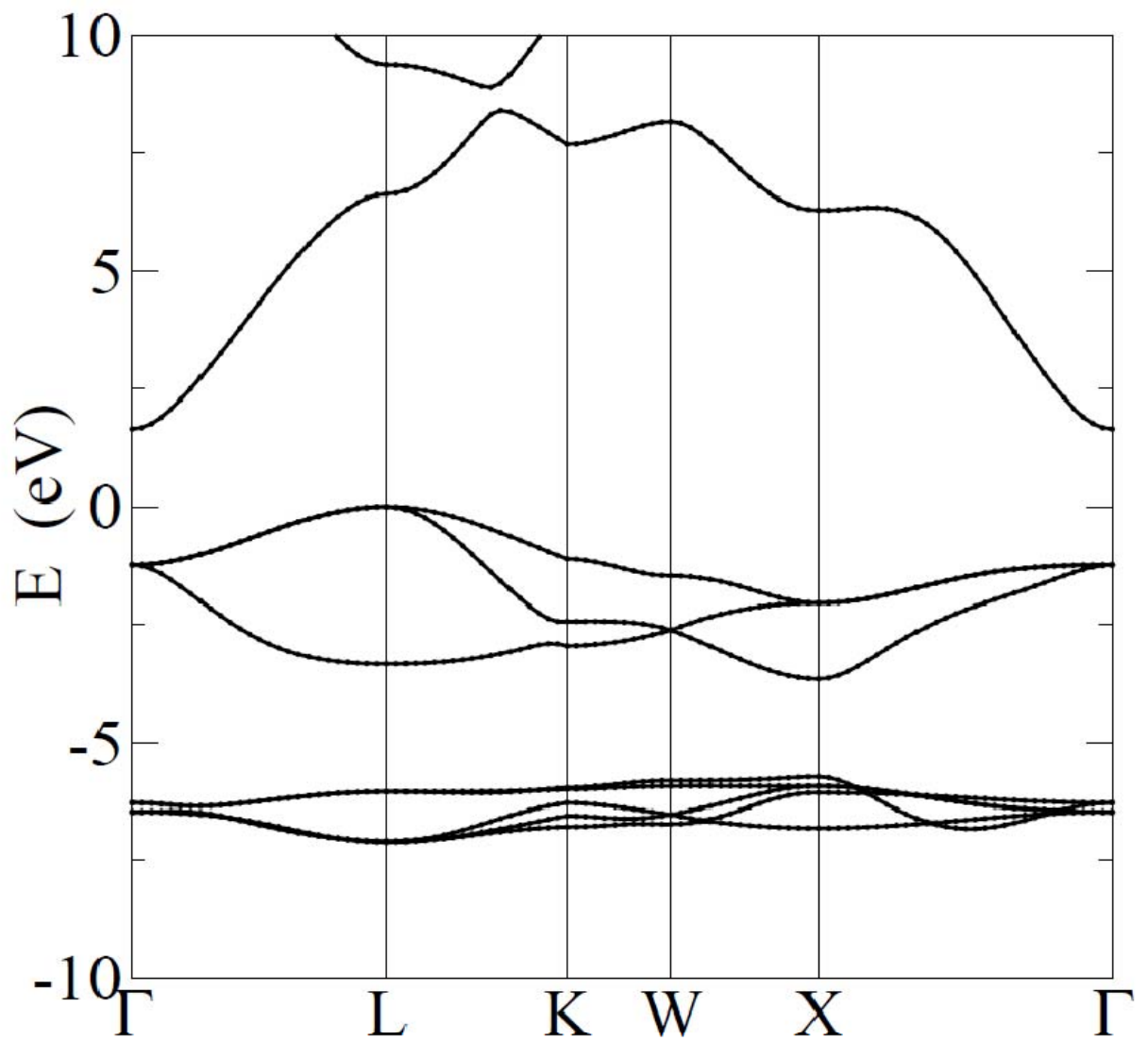


Figure 3

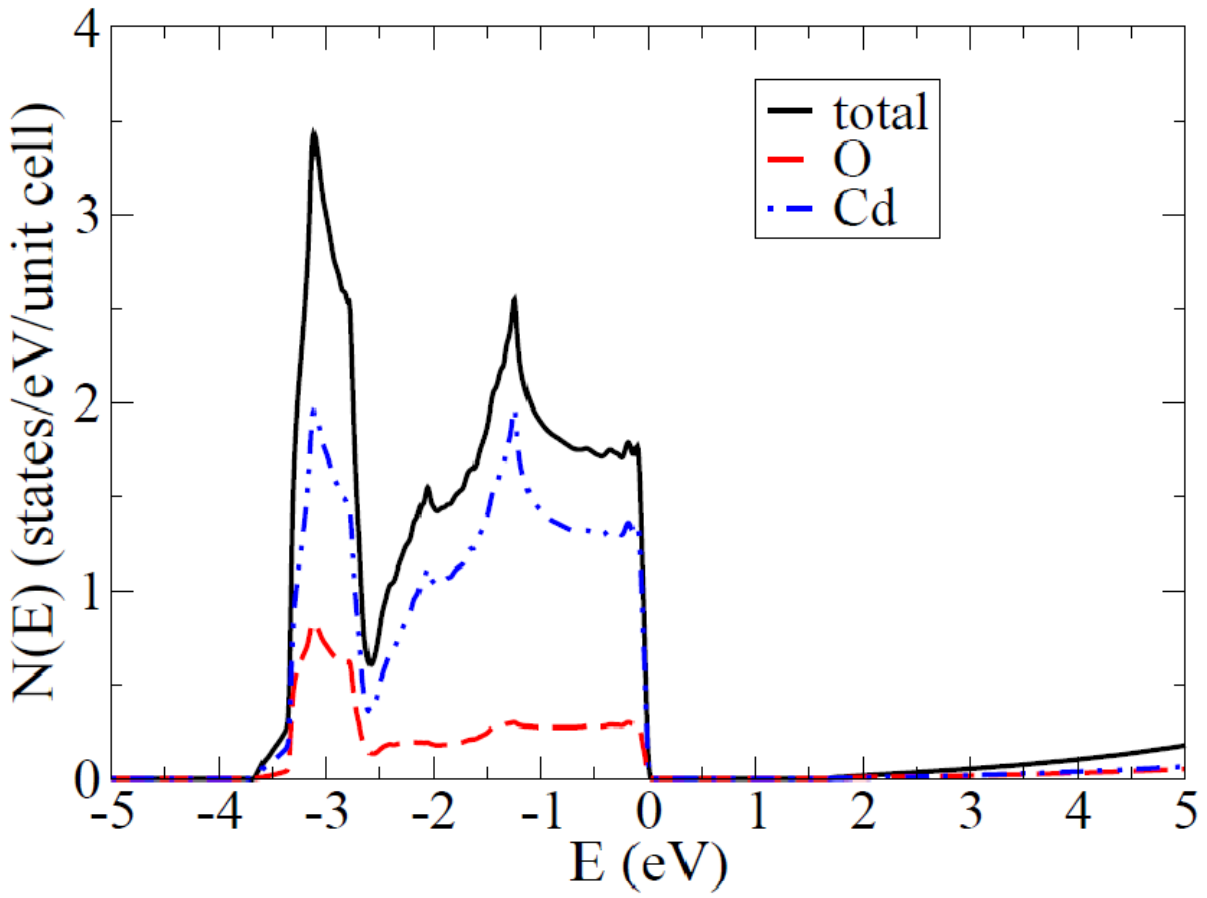


Figure 4

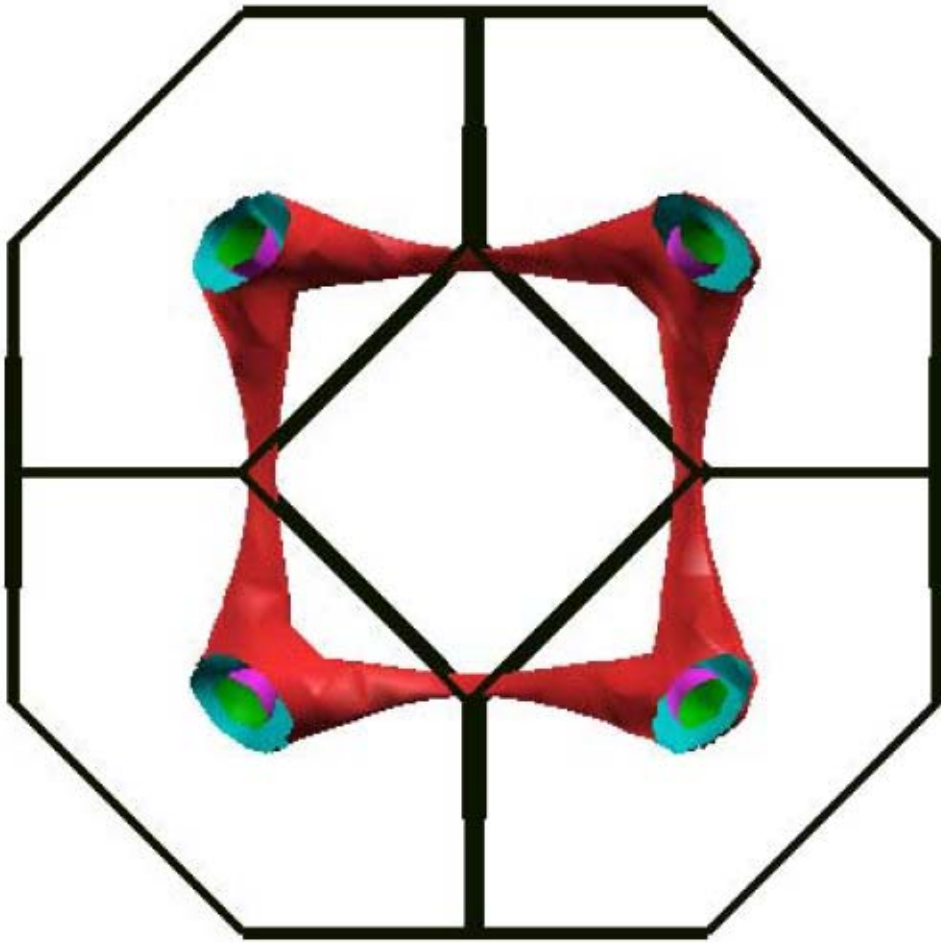


Figure 5

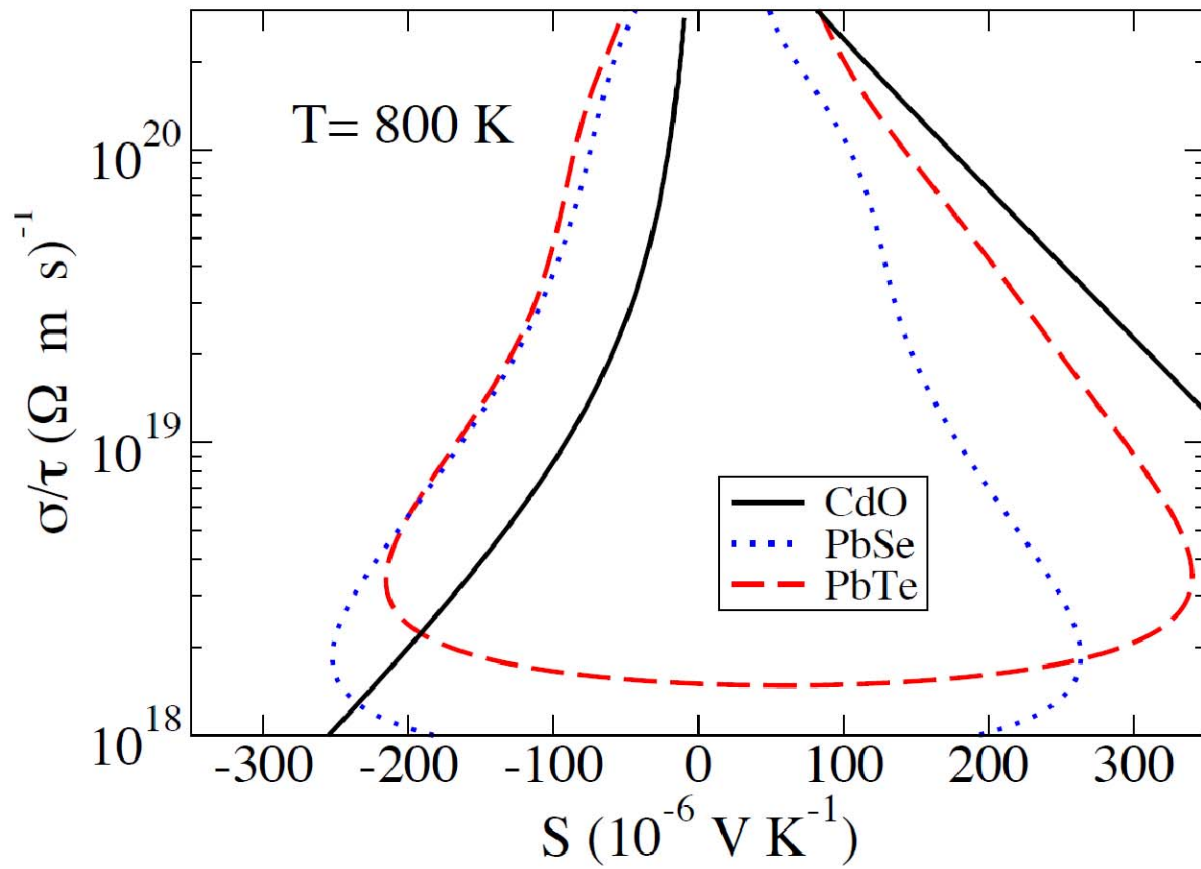


Figure 6